Separation and Purification Technology 368 (2025) 132919

Contents lists available at ScienceDirect

Separation and Purification Technology

journal homepage: www.elsevier.com/locate/seppur

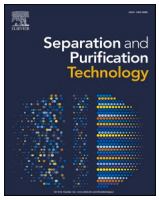

Removal of tetracycline and crystal violet from aqueous solutions by magnetic chitosan-lipid free *Chlorella vulgaris* biocomposite☆

Shabnam Mirizadeh, Alessandro Alberto Casazza *, Attilio Converti

Department of Civil, Chemical and Environmental Engineering, Genoa University, Pole of Chemical Engineering, via Opera Pia 15, I-16145 Genoa, Italy

ARTICLE INFO

Editor: B. Van der Bruggen

Keywords:
Tetracycline
Crystal Violet
Chitosan
Adsorption
Magnetic Biocomposite

ABSTRACT

The overuse and improper disposal of organic dyes and antibiotics, such as Crystal Violet (CV) and Tetracycline (TC), endanger aquatic ecosystems and water quality. In this work, a novel magnetic biocomposite was prepared by incorporating magnetite, chitosan, and residual biomass of *Chlorella vulgaris* after lipid extraction and applied for the adsorptive removal of TC and CV from water-based solutions. The highest removal of TC and CV occurred at pH 8, with the adsorption efficiency being influenced by the biocomposite dosage, the starting level of pollutants, and the time allowed for interaction. The adsorption behavior of TC aligned well with the Langmuir and Temkin adsorption isotherms, while the Langmuir model best described the CV one, indicating that this process follows monolayer-type adsorption, with the highest adsorption capacities of 864.382 mg/g for TC and 305.097 mg/g for CV. Kinetic studies showed that a pseudo-second-order model described the adsorption process, suggesting chemisorption as the primary mechanism. The thermodynamic evaluation indicated that the process was spontaneous and endothermic. This study highlights the effectiveness of the proposed biocomposite in removing antibiotics and dyes from water as an operative and sustainable adsorbent.

1. Introduction

Recently, the rapid advancement of industrialization and urbanization has led to growing concerns about water contamination, particularly from organic and emerging pollutants like synthetic dyes and antibiotics. Even trace amounts of these contaminants indeed pose serious threats to ecological systems and human health [1,2].

Synthetic dyes are used widely across industries due to their ability to form strong bonds with fabrics, resulting in vibrant, long-lasting colors that remain stable after washing and environmental exposure [3]. However, even at concentrations as low as 1 mg/L, dyes can disrupt the photosynthesis process in aquatic life by limiting light penetration. Additionally, direct contact with dyes can cause skin discoloration in humans, and inhaling them can lead to symptoms such as confusion, nausea, and vomiting [4].

Among the various hazardous dyes, Crystal Violet (CV), a triphenylmethane cationic dye, is extensively used in industries. Its strong adherence to materials, redox activity, and stability makes it valuable as a biological dye and redox indicator. Furthermore, CV is resistant to light, heat, and oxidation, making it a suitable model for studying other persistent organic pollutants in water [5].

On the other hand, numerous studies conducted over recent years have highlighted the growing concern about antibiotic contamination in aquatic systems worldwide [6,7]. The current extensive and mostly inappropriate use of antibiotics in disease treatment in humans and animals has resulted in their detection in lakes, groundwaters, rivers, and most importantly, in sources of drinking water. Indeed, these organic pollutants pose serious risks to marine and freshwater ecosystems. Antibiotics are often not completely metabolized by organisms, and hence 50–80 % of the ingested amounts are excreted and subsequently released to aquatic ecosystems [1,8]. One of the most widely used classes of antibiotics is that of Tetracycline (TC) and its derivatives, due to their affordability and broad-spectrum effectiveness. TC has been detected in substantial quantities, with over 80 % being excreted through urine within two hours of consumption. It is resistant to biodegradation and tends to bioaccumulate within the human system and other organisms via ecological feeding pathways [9].

It is therefore urgent to establish practical and effective removal methodologies for dealing with water pollution caused by dyes and antibiotics. Several treatment processes have been studied on

☆ This article is part of a special issue entitled: 'CHISA 2024 special issue' published in Separation and Purification Technology.

* Corresponding author.
E-mail address: alessandro.casazza@unige.it (A.A. Casazza).

https://doi.org/10.1016/j.seppur.2025.132919
Received 25 October 2024; Received in revised form 14 February 2025; Accepted 7 April 2025
Available online 8 April 2025

wastewater contaminated with various organic pollutants [10,11], among which adsorption has come forward because of its simplicity, economic viability, and applicability to a wide range of contaminants [12–14]. In this regard, a wide range of conventional adsorbents have been employed either in their natural or modified form to improve adsorption performance toward the effective removal of pollutants in aqueous solution. These materials include commercial activated carbons, inorganic materials such as silica gel, zeolites, and activated alumina, as well as polymeric organic ion-exchange resins. Although they possess a high degree of adsorption efficiency, their high preparation and regeneration costs have restricted their wide industrial application [15,16].

To overcome these limitations, several alternative non-conventional adsorbents have been studied, mainly derived from biological and agricultural sources. These low-cost and efficient materials include algae, bacteria, fungi, and natural fibers such as cotton [17,18]. In addition, polysaccharides such as starch, cellulose, chitosan, and alginates, along with innovative nanomaterials, have also been tested for their adsorption performance [19,20]. Their attractiveness as non-conventional adsorbents is based on their abundance, high availability, and low cost. Moreover, they often hold unique physicochemical properties and structural features which make them promising in developing complex adsorbent materials [21,22]. Based on these advancements, researchers have focused on developing composite materials that integrate multiple bio-based components to enhance adsorption efficiency and overcome individual material limitations. Among them, biopolymer-based composites have gained significant attention for their adjustable properties and high adsorption potential. For example, 3D-printed multifunctional composites based on biopolymeric matrices and waste materials have emerged as promising solutions for heavy metal remediation. These materials, with their designed structural properties and enhanced adsorption capacities, offer a sustainable and efficient approach to tackling water contamination challenges [23,24]. Additionally, biocomposites based on polylactic acid and natural fibers have been explored for use as fibrous membranes in filtration applications [25], highlighting the expanding role of biopolymer-based materials in wastewater treatment.

Beyond the adsorption performance, the economic viability is the critical factor to the industrial applicability of biocmposites. For instance, a comparative study reported that activated charcoal Norit ROX 0.8 had a cost of approximately 125.5 €/kg, and commercial ion-exchange resins are priced at 80–100 $/kg [26], whereas chitosan composites range between 7–10 €/kg. These cost differences highlight the economic advantage of biosorbents over conventional adsorbents, further emphasizing their potential as viable alternatives for wastewater treatment [27].

Among the various biocomposites explored for environmental remediation, chitosan-based materials have emerged with remarkable potential due to their unique properties and versatility.

Chitosan contains many hydroxyl and amine functional groups, which give it a cationic nature, thereby allowing its effective binding with a variety of inorganic and organic pollutants through chelation and coordination mechanisms. While chitosan exhibits several desirable characteristics, including biodegradability, biocompatibility, modifiability, and non-toxicity, some drawbacks such as solubility in acidic environments, mechanical fragility, and challenges in recovering the adsorbent after pollutant removal limit its applicability [28–30]. To overcome these limitations, researchers have focused on developing chitosan-based composites aimed at enhancing its physicochemical properties such as surface area, morphology, and mechanical strength [29].

While chitosan demonstrates strong adsorption potential, the incorporation of microalgae into biocomposites offers additional advantages, including improved pollutant adsorption through different functional groups and increased surface area for adsorption. Microalgae possess unique adsorption properties due to their cell wall-containing polysaccharides and proteins, which provide active sites for pollutant adsorption [31,32]. Additionally, the presence of negative charges on the cell wall, resulting from the dissociation of various functional groups, further promotes the biosorption of positively charged contaminants [33,34].

Combining chitosan and with *C. vulgaris* into a biocomposite material creates a synergistic system able to leverage the strengths of both components [35,36]. In a previous study by Mirizadeh et al. [36], two novel biosorbents were developed consisting of chitosan, either *Arthrospira platensis or C. vulgaris,* and magnetite. These biosorbents were designed for easy separation, enabling their reuse to remove various antibiotic classes from aqueous solutions.

To include these advantages in a cost-effective solution, this study presents the characterization and efficiency of a novel biocomposite, named MCLFC, which comprises magnetite, chitosan, and lipid-free *C. vulgaris* biomass to eliminate TC and CV from aqueous solutions. This approach offers a sustainable and cost-effective alternative to conventional adsorbents by reusing waste streams. In this process, *C. vulgaris* was cultivated in winery wastewater, reducing nutrient costs and also contributing to winery waste management. The extracted lipids serve as a valuable by-product for biofuel production, while the remaining biomass is transformed into a biocomposite, lowering waste and optimizing resource efficiency.

To assess the efficiency of the MCLFC biocomposite, the effects of different experimental parameters, including pH, temperature, and pollutant concentration, on the adsorption capacity for TC and CV were investigated. Kinetic and isotherm models were applied to realize the mechanism of pollutant removal by this biocomposite. Further investigation on the magnetic biocomposite was conducted regarding its regeneration and reuse potential in order to assess the sustainability and effectiveness of the material in practical applications.

2. Materials and methods

2.1. Materials and chemicals

Medium molecular weight chitosan, Tetracycline (TC) hydrochloride, Crystal Violet (CV), and sodium tripolyphosphate (TPP) were obtained from Sigma-Aldrich (Saint Louis, MO, USA), ferrous sulfate heptahydrate and ferric chloride hexahydrate were provided from Merck (Darmstadt, Germany), acetic acid, sodium hydroxide, and hydrochloric acid were acquired from Carlo Erba Reagents (Cornaredo, MI, Italy). *Chlorella vulgaris* strain was acquired from the CCAP, located in the UK. Winery wastewater (WWW) was kindly provided by a winery cellar located in the Piemonte region of Italy [37].

2.2. Biocomposite preparation

Initially, microalgae cells were cultured in a column photobioreactor in continuous mode. The photobioreactor was operated with a working volume of 6 L, receiving a 20 % (v/v) supply of WWW in Bold Basal medium. At the end of the growth period, the microalgal biomass was harvested through centrifugation, followed by freeze-drying. The dried biomass was then subjected to lipid extraction using a 2.0:2.0:1.8 (v/v/v) mixture of methanol, chloroform, and water, following the modified Bligh and Dyer method [38], and the residual biomass was used for the biocomposite preparation. For this purpose, approximately 0.5 g of chitosan flakes was mixed into 50 mL of 1 % (v/v) acetic acid solution and heated to 80 °C, under continuous stirring overnight. Afterward, 0.5 g of dried, lipid-extracted *C. vulgaris* powdered biomass was mixed and stirred for one hour at room temperature to ensure a homogenous biomass distribution. Next, 12 mL of 10 mg/mL TPP solution was added to cross-link the mixture, which was stirred for 15 min. After adding a solution of Fe^{2+} and Fe^{3+} (0.001 mol:0.002 mol) and dispersing it for 5 min with an ultrasonic in a water-filled, NaOH (3 N) was gradually added while stirring to adjust the pH to 11. The obtained suspension was

magnetically separated and rinsed multiple times with ultra-pure water. The final magnetic biocomposite, called MCLFC, was dried at 50 °C for 24 h, then ground, sieved with a mesh size of less than 500 μm, and reserved for future use. A graphical representation of the biocomposite preparation process has been provided in Fig. 1.

2.3. Adsorbent characterization

The features and morphology of the biocomposite and its components were examined using scanning electron microscopy (SEM). The compounds were plated with gold layers and the images were observed at a magnification of 1000X.

A Thermo Nicolet iS50 Fourier transform infrared spectroscopy (FTIR) was employed to identify the functional groups and characterize the chemical bonds present on the surface of the adsorbent. Infrared spectra were collected within the wavenumber range of 400–4000 cm^{-1} using the Omnic Lite Software.

The point of zero charge (pHpzc) was evaluated by immersing the adsorbent in NaCl solutions (0.01 M) adjusted to pH levels between 3 and 11 [39].

2.4. Experimental procedure

A set of duplicate experiments was carried out to examine the impact of variables such as initial pH (3–11), adsorbent dosage (0.05–1 g/L), initial concentrations of TC (10–100 mg/L), and CV (5–100 mg/L), as well as temperature (25, 30, and 35 °C) on the adsorption efficiency. During the experiments, the flasks were sealed and covered to avoid photodegradation and volume changes. The collected data were analyzed to determine equilibrium isotherms, kinetics, and thermodynamic properties. The initial and residual concentrations of TC and CV were measured utilizing a UV/Vis spectrophotometer at 360 nm and 590 nm, respectively. The samples of the adsorbent were also regenerated by cycling experiments using 5 mL of 0.1 N NaOH, followed by washing with ultra-pure water to remove any remaining TC and CV and drying for subsequent reuse. The percentage removal (Y, %), adsorption capacity at time t (q_t, mg/g), and adsorption capacity at equilibrium (q_e, mg/g) were estimated using the corresponding formulas:

$$Y(\%) = \left(\frac{C_0 - C_e}{C_0}\right) \times 100 \quad (1)$$

$$q_t = \frac{(C_0 - C_t)V}{m} \quad (2)$$

$$q_e = \frac{(C_0 - C_e)V}{m} \quad (3)$$

where C_0, C_t, and C_e (mg/L) are the initial, residual, and equilibrium concentrations, respectively, m is the mass of the dried adsorbent (g), and V is the solution volume (L).

2.5. Isotherm, kinetic, and thermodynamic of adsorption process

Adsorption isotherms were analyzed through models such as Langmuir, Freundlich, Temkin, and Dubinin-Radushkevich (D-R) to explain the adsorption behavior and interaction of TC and CV onto MCLFC. The Langmuir model, presuming the formation of monolayer adsorption and consistent adsorption energy, is expressed as follows:

$$q_e = \frac{K_L q_m C_e}{1 + K_L C_e} \quad (4)$$

where q_m (mg/g) is the theoretical maximum monolayer coverage capacity, while K_L (L/mg) is the Langmuir constant that expresses the molecule affinity to the adsorption sites.

The Freundlich model describes adsorption taking place on irregular or diverse surfaces:

$$q_e = K_F C_e^n \quad (5)$$

where K_F ($mg^{1-1/n}\ L^{1/n}\ g^{-1}$) is the Freundlich constant, and n is the heterogeneity factor.

The D-R model accounts for the adsorbent pore size and distribution:

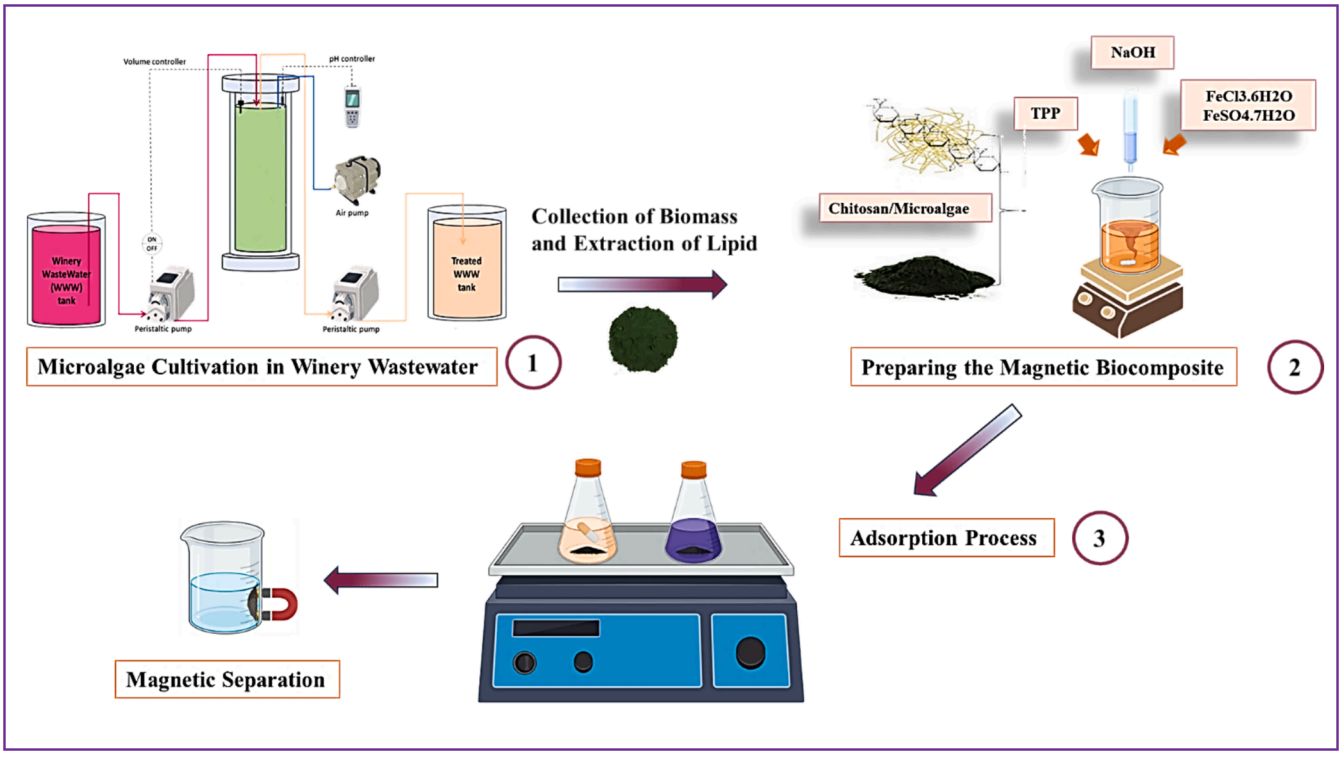

Fig. 1. Graphical representation of the biocomposite preparation process.

$$q_e = q_s \exp(-B\varepsilon^2) \quad (6)$$

where q_s (mg/g) represents the theoretical saturation capacity, B (mol^2/kJ^2) is a factor related to the mean energy of adsorption (E) (kJ/mol), and ε (kJ/mol) denotes the Polanyi potential energy. The expressions for ε and E are defined below:

$$\varepsilon = RT\ln(1+\frac{1}{C_e}) \quad (7)$$

$$E = \frac{1}{\sqrt{2B}} \quad (8)$$

The Temkin model accounts for linear decreases in the adsorption heat as the surface occupancy of the adsorbent increases:

$$q_e = \frac{RT}{b_T}\ln(A_T C_e) \quad (9)$$

where A_T (L/mg) denotes the constant of equilibrium association, and b_T (J/mol) is a factor associated with the energy of adsorption.

The pseudo-first-order (PFO) (Eq. (10)), Pseudo-Second-Order (PSO) (Eq. (11)), and Weber-Morris (WM) (Eq. (12)) models used to assess adsorption kinetics:

$$\ln(q_e - q_t) = \ln q_e - k_1 t \quad (10)$$

$$\frac{t}{q_t} = \frac{1}{k_2 q_e^2} + \frac{1}{q_e}t \quad (11)$$

$$q_t = k_i t^{0.5} + C_i \quad (12)$$

where k_1 (1/min) and k_2 (g/mg·min) denote the rate constants for the PFO and PSO models, respectively, while k_i (mg/g.min$^{0.5}$) corresponds to the intraparticle diffusion rate constant and C_i (mg/g) accounts for the boundary layer effect.

Thermodynamic studies were conducted at distinct temperatures (25, 30, and 35 °C) under optimized setting to evaluate the key characteristics, including the standard Gibbs free energy changes (ΔG°, kJ/mol), enthalpy (ΔH°, kJ/mol) and entropy (ΔS°, J/mol.K), which were calculated as follows:

$$\Delta G^\circ = -RT\ln K_D \quad (13)$$

$$\Delta G^\circ = \Delta H^\circ - T\Delta S^\circ \quad (14)$$

where K_D (q_e/C_e) is the distribution coefficient.

3. Results and discussion

3.1. Characterization of biocomposite and its components

The morphological characteristics of the materials, namely, *Chlorella vulgaris* biomass both before and after lipid extraction, chitosan combined with lipid-extracted *C. vulgaris* biomass, and the magnetic biocomposite of chitosan with lipid-extracted *C. vulgaris* biomass, were examined by SEM. According to the images illustrated in Fig. 2, *C. vulgaris* had a smooth, uniform surface prior to lipid extraction, consistent with its natural cell structure, which, however, became more porous and fragmented after extraction, leading to an overall increase in surface irregularities. On the other hand, the magnetic composite showed a much more complex, matrix-like, and heterogeneous surface structure. It is likely that the small magnetic iron oxide particles deposition resulted in the formation of irregular protrusions, and that this

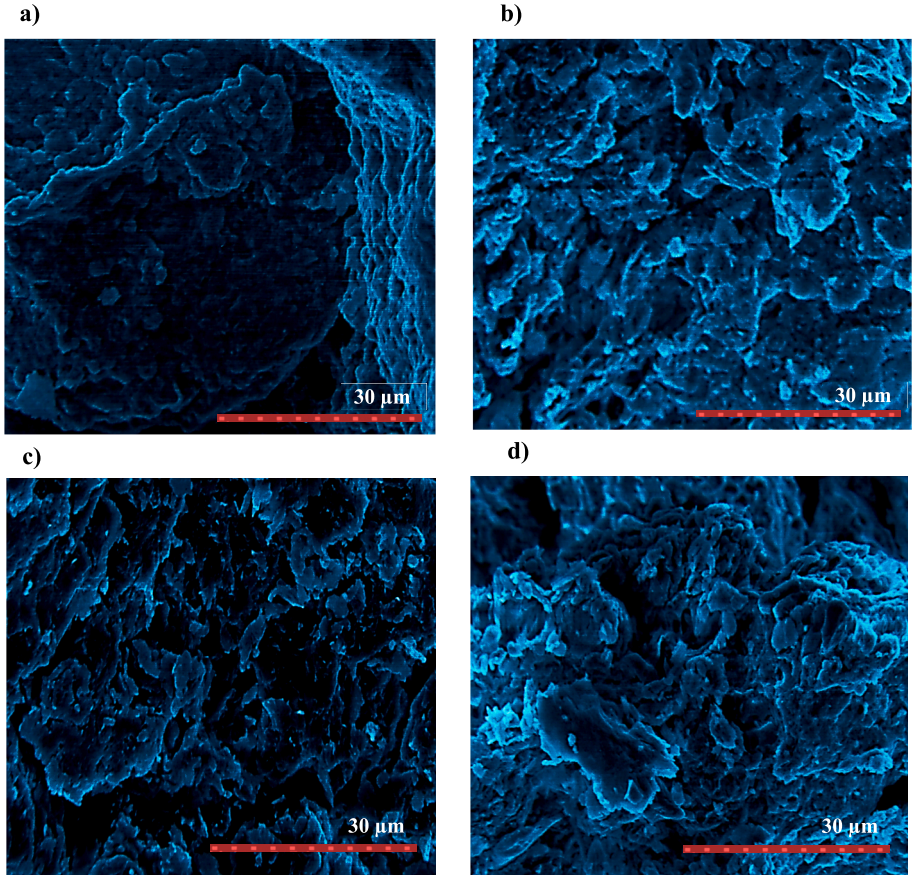

Fig. 2. SEM images at a magnification of X1000 showing (a) *C. vulgaris* biomass; (b) *C. vulgaris*-lipid extracted biomass; (c) chitosan/*C. vulgaris*-lipid extracted biomass; (d) magnetic biocomposite.

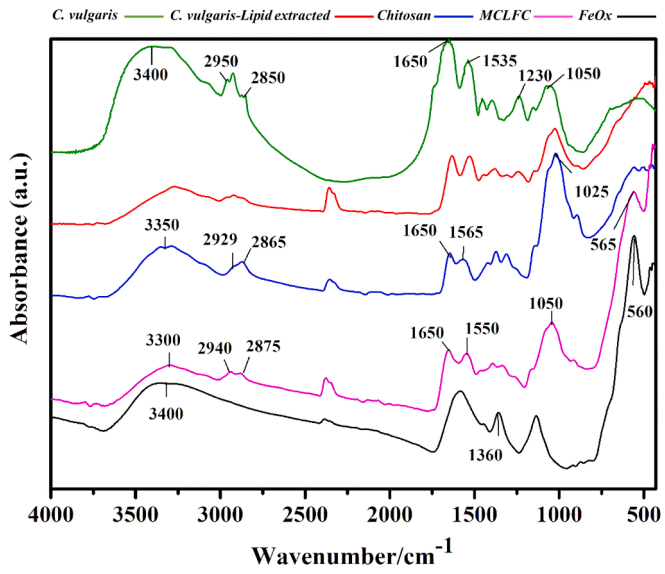

Fig. 3. FTIR spectra of *C. vulgaris* biomass, *C. vulgaris*-lipid extracted biomass, chitosan, FeOx, and Magnetic Biocomposite (MCLFC).

rough and irregular surface increased the surface area and provided more binding sites, improving the adsorption capacity of molecules.

Functional groups present in the materials were subsequently analyzed by FTIR spectroscopy.

As shown in Fig. 3, a broad peak in the range of 3400–3500 cm^{-1} was observed in all spectra, which can be attributed to water absorbed on the sample surface, hydroxyl functionalities (—OH) found mainly in microalgal cell walls and chitosan, and amine (NH_2) groups from chitosan [40].

The chitosan spectrum displayed peaks near 2870 and 2925 cm^{-1}, which are associated with the C—H bonds stretching vibrations in aliphatic groups and the main polymer chain of chitosan, respectively, the peak near 1640 cm^{-1} probably originated from the stretching vibration of C═O bond in the amide I group in the remaining acetylated glucosamine residues in chitin. The peak near 1560 cm^{-1} could be assigned to the stretching vibration of the C—N bond and the N—H bending bond in the amide II group, and the peak near 1120 cm^{-1} to the stretching vibration of the C—O—C in glycosidic linkages between glucosamine residues [36,40].

In *C. vulgaris*, the peak in the range of 2950–2850 cm^{-1} can be ascribed to the symmetric and asymmetric stretching vibrations of C—H bonds from fatty acids, while the peaks near 1620 and 1650 cm^{-1} to the stretching vibrations of the C═C bond in unsaturated fatty acids and C═O group in protein amide I, respectively. In addition, the peak near 1500 cm^{-1} is possibly because of the bending of the N—H bond and stretching vibrations of the C—N bond in protein, that near 1220 cm^{-1} to the asymmetric stretching of P═O in compounds that contain phosphate, primarily phosphodiesters, and the one near 1020 cm^{-1} to the C—O—C bond in polysaccharides. Following lipid extraction, a notable reduction in the intensity of the C—H stretching groups (2950–2850 cm^{-1}) and P═O stretching (1230 cm^{-1}) was noted, confirming the removal of lipids from the biomass [41].

The FTIR spectrum of the magnetic biocomposite displayed key characteristic peaks associated with both chitosan and the lipid-extracted *C. vulgaris* components, as well as an additional peak related to the Fe—O stretching band near 565 cm^{-1}, confirming the successful incorporation of magnetic nanoparticles into the biocomposite (MCLFC).

The pHpzc, which plays a key role in adsorption efficiency, was shown to be 6.5 for MCLFC. At solution pH values below the pHpzc, the biocomposite surface is predominantly positively charged, enhancing its attraction to negatively charged species. Conversely, the surface becomes mostly negatively charged at pH values higher than the pHpzc, which promotes the positively charged ions or molecules adsorption.

3.2. Effects of various factors on adsorption

3.2.1. Effect of pH

The effect of pH on the adsorption process was first examined. As is well known, the solution's pH is crucial in adsorption as it influences the adsorbent's surface charge and alters the speciation of the dissolved pollutant [28,42]. As shown in Fig. 4, the efficiency of Tetracycline (TC) removal increased as the initial pH (pH_i) was raised from 3 to 8, but it declined under more alkaline conditions. Consequently, the maximum TC removal (90.3 %) occurred at a pH_i of approximately 8 after 2 h of contact time.

According to Althumayri et al. [43], TC has a number of ionizable groups that produce distinct charge states and have pKa values of 3.3, 7.7, and 9.7. At pH values under 3.3, TC carries a positive charge (TCH_3^+); within the pH_i range of 3.3 to 7.7, it exists in a neutral state ($TCH_2^{\pm}$); between pH_i 7.7 and 9.7, it is negatively mono-charged (TCH^-), and at pH_i values above 9.7, it is fully negatively charged (TC^{2-}).

Under strongly acidic conditions, the positive charge on MCLFC repelled the positively charged TC molecules, hindering the adsorption process. As the pH_i increased to 7.7, the concentration of TC molecules carrying a positive charge reduced, allowing for the adsorption of zwitterionic TC molecules through the ion exchange mechanism. Simultaneously, the reduction in electrostatic repulsion between TC and MCLFC facilitated their interaction. Remarkably, the highest TC removal efficiency was recorded at pH_i of 8, where the adsorbent surface carried a negative charge and TC molecules presented as monovalent anions. Mirizadeh et al. [36] noted that increasing pH from 3 to 8 resulted in an 86.5 % TC removal efficiency using a biosorbent comprised of magnetite, chitosan, and *Arthrospira platensis* biomass. Similarly, a study by Ahamad et al. [44] revealed that the maximum TC adsorption capacity of a chitosan-based magnetic nanocomposite occurred at pH_i of 8. Such an effective adsorption can be ascribed to the robust π-π interactions and Van der Waals forces between the adsorbent surface and the benzene rings of TC molecules. However, further increases in pH_i led to a reduction in adsorption yield, likely due to strong repulsive forces.

For CV, a cationic dye, the removal efficiency also increased with increasing pH_i, achieving a maximum value of approximately 85.2 % at a pH_i range of 7–8. This increase was probably attributed to the adsorbent's surface's excess of OH^- ions, which increased the attraction of positively charged CV molecules. In contrast, the presence of H + ions at low pH caused the MCLFC surface to become positively charged. These ions competed with CV molecules, leading to a reduction in the adsorption effectiveness. The study was limited to a pH_i of 8, as higher pH_i values caused CV degradation.

3.2.2. Impact of adsorbent dosage

To ascertain the optimal biocomposite quantity for achieving the highest capacity of adsorption, the effect of the adsorbent dosage (*m*) on both removal efficiency and adsorption capacity was studied by varying it between 0.05 g/L and 1 g/L. As shown in Fig. 5, a progressive increase in *m* led to a significant improvement in removal efficiency, which reached maximum values of 89.51 % for TC and 95 % for CV. However, despite the higher removal efficiency, the adsorption capacity exhibited

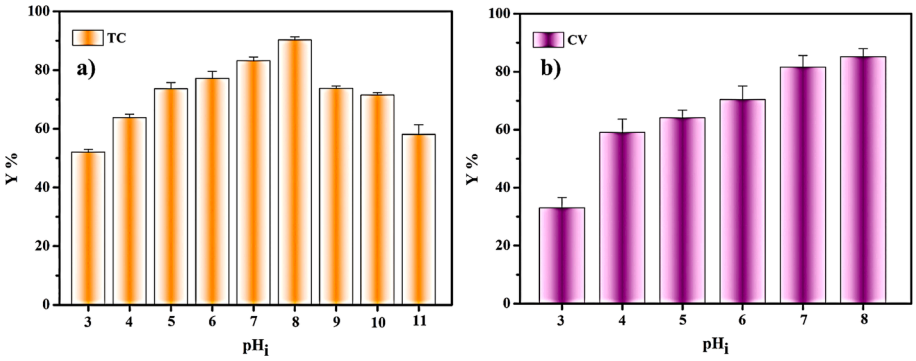

Fig. 4. Initial pH (pH_i) effect on the yield (Y) of a) Tetracycline (TC) and b) Crystal Violet (CV) adsorption onto magnetite/chitosan/*C. vulgaris*-lipid extracted adsorbent. Experimental conditions: initial TC concentration: 30 mg/L, initial CV concentration: 10 mg/L, adsorbent dosage: 0.05 g/L, temperature 298 K, and contact time: 180 min.

a decline for $m > 0.05$ g/L, which can be ascribed to the excessive increase in unoccupied binding sites, resulting in lower efficiency in the use of the adsorbent surface area per unit mass [24,29]. The maximum TC and CV adsorption capacities were found to be 367.901 mg/g (58.7 %) and 167.02 mg/g (3 %), respectively. These results are qualitatively similar to those for the adsorption of sulfamethoxazole onto a chitosan-biochar composite using adsorbent dosages in the range of 1–20 g/L [45]. Many studies that focused on the effect of adsorbent dosage have often prioritized simply increasing the amount to maximize pollutant removal. However, it should be noted that, while using higher dosages may improve performance, it can also lead to economic downsides and practical issues such as clumping and blocking of active sites.

3.2.3. *Impacts of initial pollutant level and contact time*

Fig. 6 illustrates the changes in the adsorption capacity at different initial concentrations of TC and CV. This investigation is valuable given the wide range of pollutant concentrations found in industrial wastewater.

When the concentration of TC was raised from 10 to 100 mg/L, the adsorption capacity along the time (q_t) progressively increased and reached a maximum value of 730 mg/g, with only slight variations observed above 80 mg/L. A similar trend was noted for CV, which achieved a maximum q_t value of 270 mg/g at 100 mg/L. This increase in adsorption capacity at higher initial concentrations of TC and CV can be attributed to the enhanced driving force between the two phases [46].

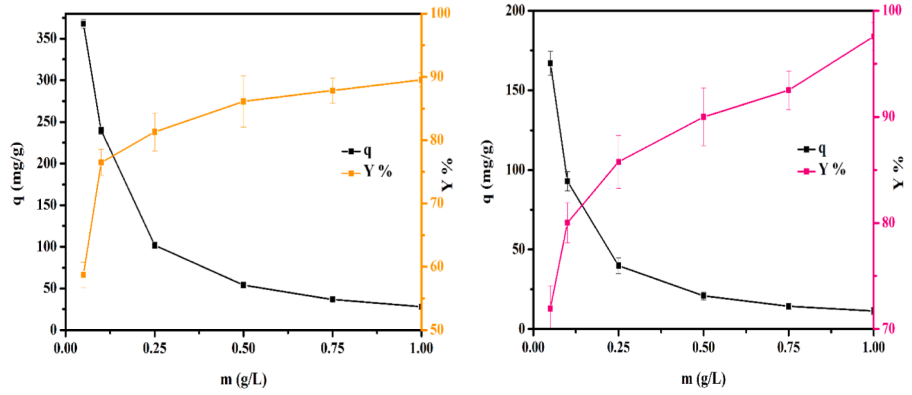

Fig. 5. Biocomposite quantity effects on the removal efficiency (Y) and adsorption capacity (q); a) tetracycline, initial concentration: 30 mg/L and b) crystal violet, initial concentration: 10 mg/L; pH: 7.5–8, contact time: 1 h.

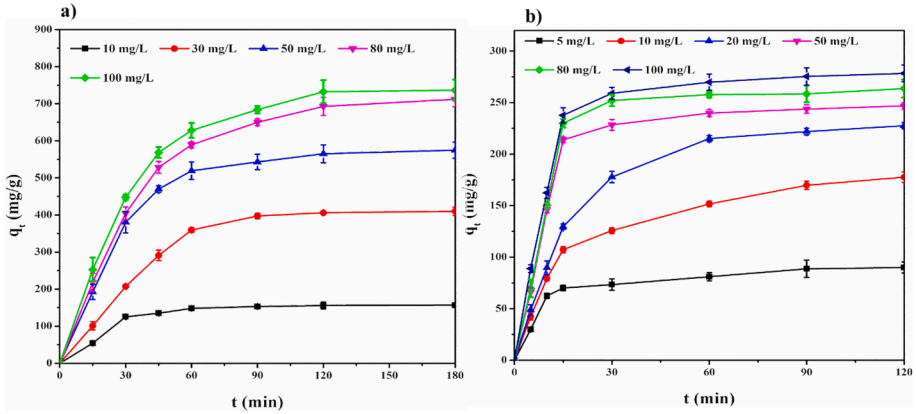

Fig. 6. Effects of initial concentration of (a) tetracycline and (b) crystal violet on the biocomposite adsorption capacity (q_t) over time (t).

Regarding contact time, a quite important factor in practical applications, q_t for TC increased rapidly during the initial 60 min, and adsorption reached equilibrium after 120 min. For CV, q_t rose quickly during the initial 15 min, followed by a gradual decline in the rate of adsorption, eventually reaching equilibrium around 90 min.

It was also noted that the starting pollutant concentration (C_0) did not significantly influence the duration required to achieve adsorption stability, with the exception of the 10 mg/L TC concentration, reaching equilibrium in 60 min. As the increase in contact time, the adsorption of both TC and CV gradually slowed down until saturation was achieved. This behavior can be assigned to a decrease in the number of accessible adsorption sites and the presence of repelling interactions between the bulk phase and the solute molecules, a fact that was confirmed in many studies [36,47,48].

Although the present study evaluated the efficiency of MCLFC biocomposite for the removal of TC and CV at the laboratory scale, its possible application in real wastewater treatment appears highly promising. This potential is supported by studies on similar materials, such as magnetic chitosan and microalgae-based adsorbents, which have shown effectiveness in treating real industrial effluents.

Basically, the efficiency of adsorption for such materials depends greatly on the kind of industrial effluent, concentration of contaminants, and presence of other organic and inorganic competitors. For instance, Kyzas et al. [27] investigated the adsorption of mixtures of dyes onto chitosan beads coming from industrial dyeing effluent. The adsorption capacity resulted in 466 mg/g for synthetic effluent and 447 mg/g for real effluent, with only a slight decrease when passing from controlled to real conditions.

Moreover, when compared to commercial activated carbon, which exhibited adsorption capacities of 542 mg/g and 521 mg/g for synthetic and real effluents, respectively, the chitosan-based material still demonstrated competitive performance.

Similarly, Nasiri et al. [49] evaluated a CuCoFe2O4@Chitosan biocomposite for TC removal and observed a reduction in efficiency from 93.07 % in synthetic samples to 67 % in real samples. This decrease was likely due to the presence of soluble organic matter and competing pollutants. Nevertheless, the material still exhibited an appreciable removal capacity. Microalgae-based adsorbents have also been applied to treat complex effluents. For example, a study on magnetic *Spirulina*-based adsorbents reported a 98 % removal efficiency in textile dyeing wastewater, showing that microalgae-based materials can be effective in real-world applications [50].

These observations therefore suggest that the MCLFC biocomposite, which incorporates both chitosan and microalgae, holds potential for real-world wastewater treatment. While its performance in complex wastewater systems is expected to be comparable to that of similar materials, future research should focus on testing the MCLFC biocomposite in real industrial effluents to fully establish its practical applicability.

3.2.4. Regeneration of the biocomposite

The regeneration and reusability of MCLFC were evaluated over four consecutive adsorption–desorption cycles using 0.1 N NaOH as the desorbing agent. The regeneration efficiency of the biocomposite gradually decreased with each cycle, indicating a decline in the material's adsorption capacity towards both TC and CV (Fig. 7). Specifically, after four cycles, the adsorption capacity decreased by 12 % for TC and 15 % for CV. Such a reduction could be attributed to several factors. Repeated exposure to the alkaline regenerating agent (NaOH) may have caused partial degradation or structural alteration of the chitosan or *C. vulgaris* components of the composite. Additionally, the loss of active sites, including amino and hydroxyl groups responsible for electrostatic interactions and hydrogen bonding, may have contributed to the decline in adsorption efficiency.

In comparison to other adsorbents, various regeneration techniques have been investigated in the literature, including chemical (acids, bases, salts, and organic solvents), thermal, and microwave-assisted techniques. Among them, acid and base regeneration methods are the most commonly used due to their simplicity and effectiveness. However, the use of acids may result in adsorbent degradation, while thermal methods can be energy-intensive. In the case of MCLFC, 0.1 N NaOH as a regenerating agent aligns with the broader trend of using alkaline solutions for chitosan-based materials since they can effectively desorb contaminants without compromising material stability.

Several studies have investigated the regeneration of chitosan- and microalgae-based adsorbents using different approaches. For instance, Zheng et al. [51] used 1 M HCl to regenerate a magnetic chitosan composite and achieved a desorption efficiency of over 90 % after five cycles of TC adsorption–desorption. Similarly, in another study on CV adsorption, the regeneration efficiency decreased by around 20 % after six cycles using 0.1 M HCl [52]. Liu et al. [53] reported that the regeneration of TC from the ethylenediamine-modified magnetic chitosan using 0.1 M NaOH kept the regeneration efficiency at 76.2 % after four cycles.

These findings align with the observed decline in MCLFC's adsorption capacity, suggesting that repeated exposure to chemical regenerants, whether acidic or alkaline, can gradually reduce efficiency due to structural changes or the depletion of active sites. Other chemical desorption methods include salt and solvent-based regeneration. He et al. [54] used a 1 M NaCl solution to regenerate a Konjac glucomannan-GO-chitosan-sodium alginate composite for the adsorption of ofloxacin, TC, and sulfadiazine, achieving removal yields above 70 % after five cycles. Ahamad et al. [44] used 40 % methanol to regenerate a chitosan/thiobarbituric acid/malondialdehyde-Fe_3O_4 composite for TC desorption, reaching 95 % desorption efficiency after five cycles. However, methanol's toxicity requires careful handling, which may limit its practical use. These studies highlight the trade-offs between desorption efficiency, material stability, and environmental safety when choosing a regeneration method.

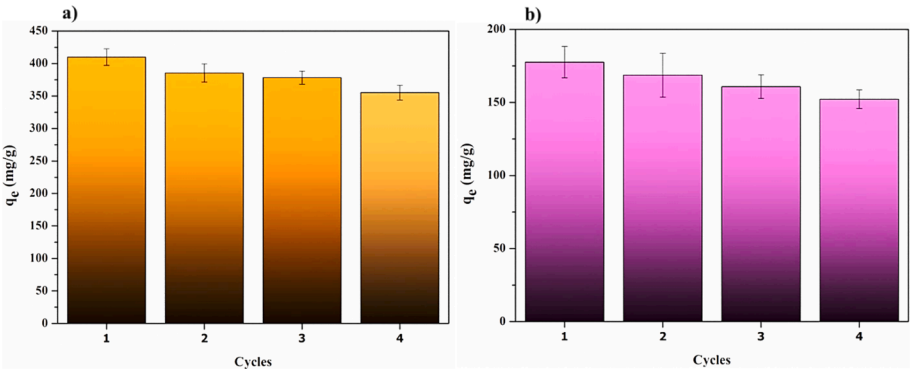

Fig. 7. Impact of four consecutive reuses of the biocomposite on its equilibrium adsorption capacity (q_e) towards a) tetracycline, and b) crystal violet.

Microwave-assisted regeneration has also been explored as an alternative technique to reduce chemical consumption. This technique quickly and uniformly heats the adsorbent, enhancing desorption by breaking adsorbate-adsorbent bonds effectively [55]. Mirizadeh et al. [36] applied microwave-assisted treatment to magnetic chitosan-microalgal adsorbents, enabling reuse over four cycles with negligible adsorption capacity loss (7 % for TC, 4 % for ciprofloxacin, and 9 % for amoxicillin).

In general, various regeneration methods have been successfully applied to the adsorbents, each with their respective advantages and limitations. Each method is chosen according to different criteria such as desorption efficiency, stability of materials, environmental impact, and operational feasibility.

3.3. Adsorption isotherms, kinetics, and thermodynamics

Isotherm models assist in understanding the adsorption mechanism, which assumes that the adsorption of adsorbate depends on the equilibrium concentration. For this purpose, the data obtained in this study were analyzed using the Langmuir, Freundlich, Temkin, and Dubinin-Radushkevich (D-R) models to give details about the adsorption behavior. The fitting results obtained from all these models are given in Table 1, and the fitting curves are illustrated in Fig. 8.

The Langmuir model describes monolayer adsorption occurring on a uniform surface with a limited number of adsorption sites. The maximum adsorption capacity for TC (q_m) was 864.382 mg/g, which indicates a high affinity between the adsorbent and the antibiotic. The high value of the determination coefficient ($R^2 = 0.998$) confirms the excellent fit of the data to this model. For CV, the maximum capacity (305.097 mg/g) was significantly lower than for TC but still suggests a good adsorption performance, and the R^2 value of 0.964 indicates a reasonably good fit of results to the model. The Langmuir constant ($K_L =$ 0.795 L/mg) for CV was much higher than that for TC ($K_L = 0.096$ L/mg), indicating a higher affinity for CV at low concentration. This result could be attributed to the cationic nature of this dye and the negatively charged surface functional groups on the biocomposite that enhanced electrostatic interactions.

According to the Freundlich model, adsorption occurs on non-uniform surfaces, and this model provides insight into surface heterogeneity and adsorption intensity, in terms of the n parameter. An n value within the range of 0 to 1 suggests that the removal of adsorbate is favorable, if n equals 1, the adsorption process represents a linear relationship without any interactions among adsorbed molecules, while an n value exceeding 1 indicates less favorable and more difficult adsorption [56]. For TC and CV, n was 0.3709 and 0.169, respectively, which suggests favorable adsorption in both cases, with the R^2 values indicating a better fit for TC (0.949) than for CV (0.846).

The D-R isotherm provides information about the adsorption energy and facilitates the differentiation of physical and chemical adsorption mechanisms. For TC, the adsorption capacity (q_s) was estimated as 718.669 mg/g. The adsorption energy estimated by the model ($E =$ 0.227 kJ/mol) was well lower than 8 kJ/mol, which suggests that the predominating mechanism was physical adsorption [57]. However, the relatively low R^2 value (0.841) indicates that this model did not fit satisfactorily the TC adsorption data. For CV, the value of q_s (290.163 mg/g) was much lower, while that of E (1.409 kJ/mol) was much higher than for TC, thus suggesting that the mechanism of dye adsorption may include more complex processes, possibly involving physical and weak chemical interactions.

The Temkin model accounts for the linear decrease in adsorption energy due to adsorbate-adsorbent interactions [58]. For TC, the values of the b_T parameter (14.033 J/mol) and the equilibrium binding constant ($A_T = 1.116$ L/mg) suggest moderate interactions between the adsorbent and the antibiotic given the good fitness ($R^2 = 0.994$), while a value of b_T more than 4 times higher for CV (62.525 J/mol) suggests stronger adsorbate-adsorbent interactions. However, the unsatisfactory value of R^2 for CV (0.883) indicates that, although the Temkin model gives some valuable information about the adsorption mechanism, it may not be as accurate for dyes as it is for antibiotics.

To compare these results with those recently reported in the literature, maximum adsorption capacities for TC, and CV adsorption onto different chitosan- and microalgae-based adsorbents are shown in Fig. 9. For TC adsorption, MCLFC (864.4 mg/g) and MCC (831.1 mg/g) had the highest adsorption capacity, far beyond those of ZIF-8-chitosan (495 mg/g) and magnetic chitosan (230.7 mg/g) composite. MCLFC also showed a high adsorption capacity for CV adsorption, 305.1 mg/g, compared to adsorbents like chitosan aerogel at 8.1 mg/g and bentonite-chitosan nanocomposite at 113 mg/g. This indicates that the modified MCLFC has outstanding performance and promising applications in wastewater treatment.

Adsorption kinetics helps analyze the rate of adsorption and efficacy of the adsorbent, which is useful in designing batch adsorption systems and optimizing operational parameters for large-scale facilities [75]. For this purpose, the adsorption kinetics of both TC and CV were evaluated by applying three well-known kinetic models, PFO, PSO, and WM models, with their plotted curves illustrated in Fig. 10 (b–d) and corresponding kinetic parameters are listed in Table 2.

Based on the results of Table 2, the values of R^2 for the PSO model (0.993–0.997) were higher than those of the PFO one (0.985–0.923) when referring to experimental initial TC and CV concentrations up to 50 mg/L, which suggests that the mechanism of adsorption is primarily controlled by chemisorption, involving the absorbent and adsorbate sharing or exchanging electrons, rather than physical adsorption [28]. This is consistent with a wide range of studies on the adsorption of antibiotics and dyes, in which chemisorption is usually observed as a controlling mechanism due to interactions between the functional groups on the molecules and the adsorbent surface sites [72,76–78]. Accordingly, the equilibrium adsorption capacities calculated from the fitting by the PSO model ($q_{e,cal}$) were more similar to the experimental ones ($q_{e,exp}$).

For CV, the rate constants of the PSO model were larger than for TC, pointing to a quicker adsorption phenomenon. The faster adsorption of CV can be ascribed to the smaller size of its molecules and the comparably higher reactivity of their cationic form, which enhance chemisorptive interactions with the negatively charged adsorbent surface. It is worth mentioning, however, that the R^2 values of the PFO model for adsorption of both TC and CV were all > 0.900, indicating that a physical adsorption process may have also occurred in the system.

Even though the PSO model provided the best overall fit, the WM intraparticle diffusion model was also applied to check whether diffusion within the pores of the adsorbent played an important role [58,79]. The WM model suggests multistage adsorption for both TC and CV since the fitted lines did not pass through the origin point, corresponding to initial surface adsorption, followed by diffusion into the pores, and

Table 1
Isotherm model coefficients and determination coefficients (R^2) for Tetracycline (TC) and Crystal Violet (CV) adsorption onto the magnetic biocomposite.

Model	Parameters	Target contaminants	
		TC	CV
Langmuir	q_m (mg/g)	864.382	305.097
	K_L (L/mg)	0.0963	0.795
	R^2	0.998	0.964
Freundlich	n	0.3709	0.169
	K_F ($mg^{1-1/n}\ L^{1/n}\ g^{-1}$)	168.376	152.04
	R^2	0.949	0.846
D-R	q_s (mg/g)	718.669	290.163
	B $(mol/kJ)^2$	9.695	0.253
	E (kJ/mol)	0.227	1.409
	R^2	0.841	0.949
Temkin	b_T (J/mol)	14.033	62.525
	A_T (L/mg)	1.116	35.804
	R^2	0.994	0.883

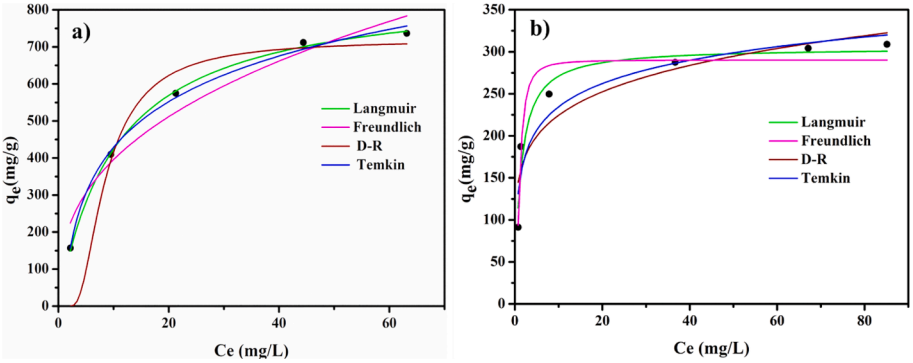

Fig. 8. Isotherms of (a) tetracycline and (b) crystal violet onto the magnetic biocomposite.

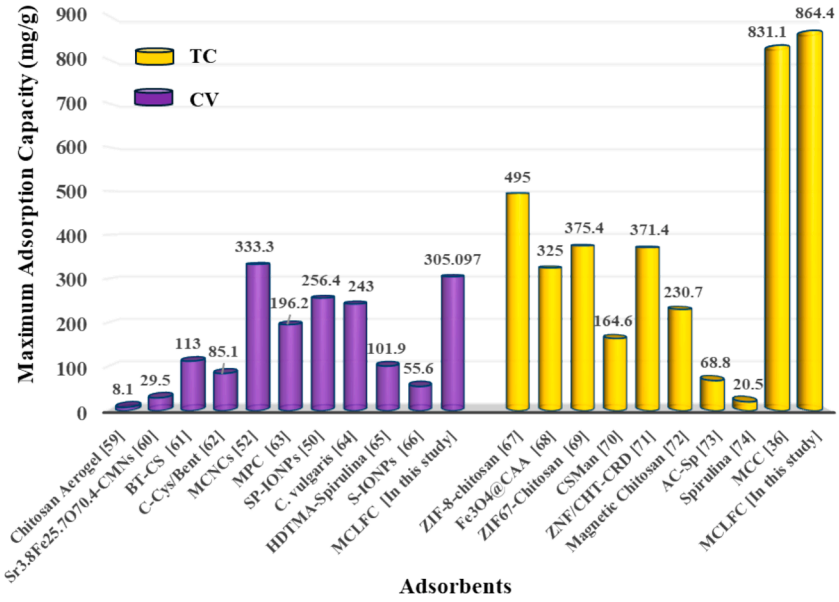

Fig. 9. Maximum adsorption capacities for Tetracycline (TC) and Crystal Violet (CV) adsorption onto various chitosan- and microalgae-based adsorbents. (CMNs: Chitosan magnetic microparticles, BT-CS: Bentonite-chitosan, CS-Cys/Bent: Chitosan-modified L-cysteine/bentonite, MCNCs: Magnetic chitosan, MPC: Magnetic pectin-*C vulgaris*, SP-IONPs: Iron oxide nanoparticles using *Spirulina platensis*, HDTMA: Hexadecyltrimethylammonium bromide, Fe3O4@CAA: Magnetic chitosan, CSMan: Mannose-grafted chitosan, AC-Sp: Activated carbon of *Spirulina*, MCC: Magnetic chitosan *C. vulgaris*.).

finally equilibrium. The R^2 values were relatively high in the early stages for both adsorbates, pointing to the predominance of surface adsorption at the beginning, while lower values in the later stages suggest that intraparticle diffusion became more significant as the process progressed. This inference aligns with typical chemisorption systems where quick initial binding to surface sites is followed by slower movement of adsorbate molecules into the interior pores of the adsorbent [80].

Thermodynamic studies are important for understanding energy changes associated with various processes, including adsorption, and for assessing their practical feasibility [81]. To explore this issue, ΔG° was estimated by the Van't Hoff equation using the distribution coefficient (K_D) (Eq. (13)), while ΔH° and ΔS° changes were calculated by plotting $\ln K_D$ against the reciprocal absolute temperature ($1/T$), according to Equation (14). The values of the thermodynamic parameters are summarized in Table 3.

The negative ΔG° values for both TC and CV indicate that the adsorption process onto MCLFC was spontaneous [82]. Additionally, the positive ΔH° values denote the endothermic nature of the adsorption process, meaning that the energy needed to expose active sites at higher temperatures might have exceeded the energy released during the interaction between sorbate and sorbent. This may have led to an increase in adsorption capacity as the temperature was raised [83]. Moreover, the positive ΔS° values indicate an increase in randomness and affinity at the solid/solution interface due to TC and CV adsorption [84].

4. Conclusions

This study demonstrated the successful application of a novel magnetic biocomposite composed of chitosan and lipid-free *Chlorella vulgaris* (MCLFC) biomass for the removal of Tetracycline (TC) and Crystal Violet (CV) from liquid solutions. The results highlighted the potential of this biocomposite as an effective and sustainable adsorbent for addressing water contamination caused by organic dyes and antibiotics. Experimental conditions such as pH, contact time, adsorbent dosage, and starting pollutant concentration, significantly influenced its performance as an adsorbent. Isotherm studies showed that the adsorption of TC and CV fitted well with the Langmuir model, suggesting monolayer adsorption on homogeneous surfaces. The maximum adsorption capacities were 864.38 mg/g for TC and 305.10 mg/g for CV. The adsorption process was found to follow a Pseudo-Second-Order (PSO) mechanism based on kinetic modeling, suggesting chemisorption as the predominant mechanism for both pollutants. Thermodynamic studies confirmed the spontaneous and endothermic nature of the adsorption

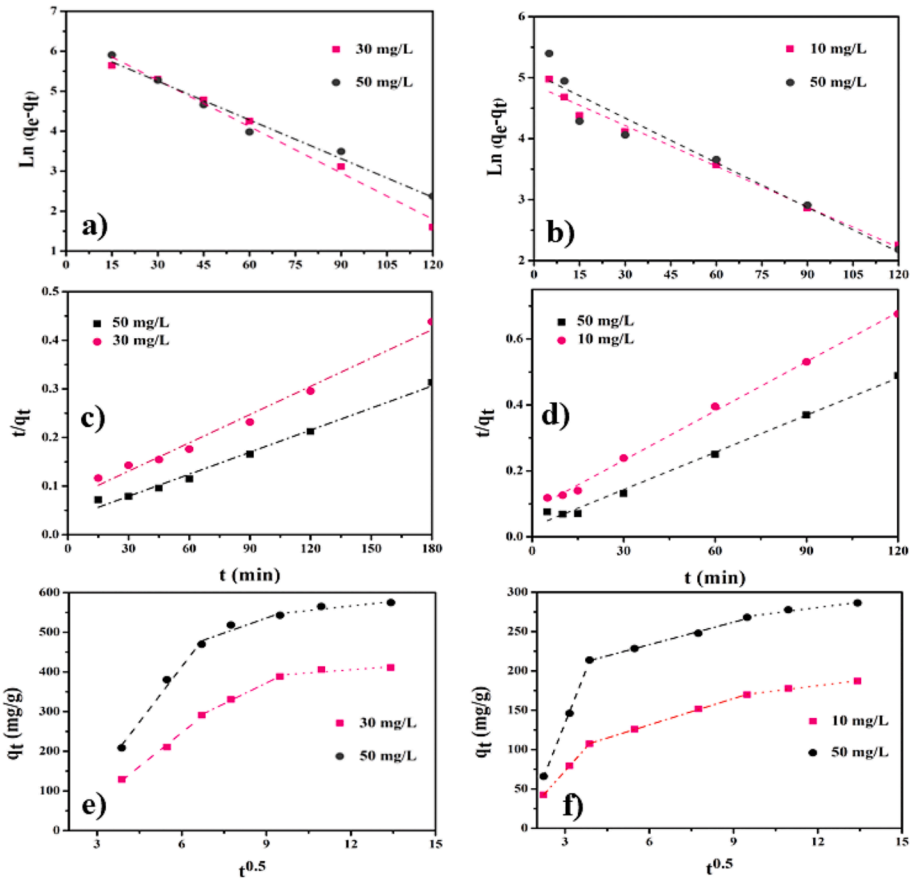

Fig. 10. Plots of adsorption kinetics for tetracycline (a,c,e) and crystal violet (b,d,f) adsorption. Models: pseudo-first-order (a,b), pseudo-second-order (c,d), and Weber-Morris (e,f).

Table 2
Kinetic models coefficients and determination coefficients (R^2) to analyze the Tetracycline (TC) and Crystal Violet (CV) adsorption onto the magnetic adsorbent.

	Parameter	TC concentration (mg/L)		CV concentration (mg/L)	
		30	50	10	50
Model	$q_{e,exp}$ (mg/g)	410.8	574.72	187.116	320.432
	$q_{e,cal}$ (mg/g)	622.43	501.433	131.739	158.7
	k_1 (1/min)	0.039	0.035	0.022	0.0244
PFO	R^2	0.985	0.972	0.983	0.923
	$q_{e,cal}$ (mg/g)	475.464	662.251	203.666	304.878
	$k_2 \times 10^3$ (g/mg·min)	0.051	0.067	0.283	0.271
PSO	R^2	0.993	0.995	0.999	0.997
	k_{i1} (mg/g.min$^{0.5}$)	56.885	92.901	39.651	90.1
	C_{i1} (mg/g)	−94.532	−144.426	−49.179	−136.5
WM	R_1^2	0.995	0.989	0.999	0.999
	k_{i2} (mg/g.min$^{0.5}$)	34.858	24.819	11.152	17.88
	C_{i2} (mg/g)	58.414	313.54	64.492	139.66
	R_2^2	0.976	0.855	0.994	0.977
	k_{i3} (mg/g.min$^{0.5}$)	5.331	7.673	4.384	2.934
	C_{i3} (mg/g)	341.5	474.258	128.64	282.25
	R_3^2	0.804	0.872	0.992	0.815

process, further supporting the feasibility of using MCLFC in practical applications. Furthermore, the biocomposite demonstrated regeneration potential, retaining high adsorption efficiencies across four consecutive adsorption–desorption cycles with declines of 12 % for TC and 15 % for CV. Overall, the MCLFC biocomposite proved to be a promising adsorbent for the efficient removal of TC and CV from contaminated water.

Table 3
Parameters of thermodynamics for tetracycline and crystal violet adsorption onto the magnetic adsorbent.

T (K)	Tetracycline			Crystal violet		
	$\Delta G°$ kJ/mol	$\Delta H°$ kJ/mol	$\Delta S°$ J/mol.K	$\Delta G°$ kJ/mol	$\Delta H°$ kJ/mol	$\Delta S°$ J/mol.K
298	− 9.23	10.11	64.9	−11.93	39.53	172.66
308	−9.88			−13.65		
318	−10.53			−15.38		

CRediT authorship contribution statement

Shabnam Mirizadeh: Conceptualization, Investigation, Formal analysis, Methodology, Writing – original draft, Writing – review & editing. **Alessandro Alberto Casazza:** Conceptualization, Methodology, Writing – original draft, Writing – review & editing, Supervision, Resources. **Attilio Converti:** Writing – original draft, Writing – review & editing, Supervision, Resources.

Declaration of competing interest

The authors declare that they have no known competing financial interests or personal relationships that could have appeared to influence the work reported in this paper.

References

[1] P. Barathe, K. Kaur, S. Reddy, V. Shriram, V. Kumar, Antibiotic pollution and associated antimicrobial resistance in the environment, J. Hazard. Mater. Lett. 5 (2024) 100105, https://doi.org/10.1016/j.hazl.2024.100105.

[2] A. Sahu, J.C. Poler, Removal and degradation of dyes from textile industry wastewater: benchmarking recent advancements, toxicity assessment and cost analysis of treatment processes, J. Environ. Chem. Eng. 12 (2024) 113754, https://doi.org/10.1016/j.jece.2024.113754.

[3] E.O. Alegbe, T.O. Uthman, A review of history, properties, classification, applications and challenges of natural and synthetic dyes, Heliyon. 10 (2024), https://doi.org/10.1016/j.heliyon.2024.e33646.

[4] J. Sharma, S. Sharma, V. Soni, Classification and impact of synthetic textile dyes on Aquatic Flora: a review, Reg. Stud. Mar. Sci. 45 (2021) 101802, https://doi.org/10.1016/j.rsma.2021.101802.

[5] G.A. Kallawar, B.A. Bhanvase, A review on existing and emerging approaches for textile wastewater treatments: challenges and future perspectives, Environ. Sci. Pollut. Res. 31 (2024) 1748–1789, https://doi.org/10.1007/s11356-023-31175-3.

[6] M.K. Nguyen, C. Lin, X.T. Bui, M.R.J. Rakib, H.L. Nguyen, Q.M. Truong, H. G. Hoang, H.T. Tran, G. Malafaia, A.M. Idris, Occurrence and fate of pharmaceutical pollutants in wastewater: insights on ecotoxicity, health risk, and state–of–the-art removal, Chemosphere 354 (2024) 141678, https://doi.org/10.1016/j.chemosphere.2024.141678.

[7] T. Fayaz, N. Renuka, S.K. Ratha, Antibiotic occurrence, environmental risks, and their removal from aquatic environments using microalgae: advances and future perspectives, Chemosphere 349 (2024) 140822, https://doi.org/10.1016/j.chemosphere.2023.140822.

[8] S. Pal, Z. Ahamed, P. Pal, Removal of antibiotics and pharmaceutically active compounds from water environment: experiments towards industrial scale up, Sep. Purif. Technol. 295 (2022) 121249, https://doi.org/10.1016/j.seppur.2022.121249.

[9] J. Antos, M. Piosik, D. Ginter-Kramarczyk, J. Zembrzuska, I. Kruszelnicka, Tetracyclines contamination in European aquatic environments: a comprehensive review of occurrence, fate, and removal techniques, Chemosphere 353 (2024) 141519, https://doi.org/10.1016/j.chemosphere.2024.141519.

[10] T. Liu, C.O. Aniagor, M.I. Ejimofor, M.C. Menkiti, K.H.D. Tang, B.L.F. Chin, Y. H. Chan, C.L. Yiin, K.W. Cheah, Y. Ho Chai, S.S.M. Lock, K.L. Yap, M.X.J. Wee, P.-S. Yap, Technologies for removing pharmaceuticals and personal care products (PPCPs) from aqueous solutions: recent advances, performances, challenges and recommendations for improvements, J. Mol. Liq. 374 (2023) 121144, https://doi.org/10.1016/j.molliq.2022.121144.

[11] H.M. Solayman, M.A. Hossen, A. Abd Aziz, N.Y. Yahya, K.H. Leong, L.C. Sim, M. U. Monir, K.-D. Zoh, Performance evaluation of dye wastewater treatment technologies: a review, J. Environ. Chem. Eng. 11 (2023) 109610, https://doi.org/10.1016/j.jece.2023.109610.

[12] R. Agarwala, L. Mulky, Adsorption of dyes from wastewater: a comprehensive review, ChemBioEng Rev. 10 (2023) 326–335, https://doi.org/10.1002/cben.202200011.

[13] L. Du, S. Ahmad, L. Liu, L. Wang, J. Tang, A review of antibiotics and Antibiotic Resistance Genes (ARGs) adsorption by biochar and modified biochar in water, Sci. Total Environ. 858 (2023) 159815, https://doi.org/10.1016/j.scitotenv.2022.159815.

[14] M. El-habacha, Y. Miyah, S. Lagdali, G. Mahmoudy, A. Dabagh, M. Chiban, F. Sinan, S. Iaich, M. Zerbet, General overview to understand the adsorption mechanism of textile dyes and heavy metals on the surface of different clay materials, Arab. J. Chem. 16 (2023) 105248, https://doi.org/10.1016/j.arabjc.2023.105248.

[15] G. Crini, E. Lichtfouse, L.D. Wilson, N. Morin-Crini, Conventional and non-conventional adsorbents for wastewater treatment, Environ. Chem. Lett. 17 (2019) 195–213, https://doi.org/10.1007/s10311-018-0786-8.

[16] M.A. Kaczorowska, D. Bożejewicz, The Application of chitosan-based adsorbents for the removal of hazardous pollutants from aqueous solutions—a review, Sustainability. 16 (2024), https://doi.org/10.3390/su16072615.

[17] M. Akhtar, M. Sarfraz, M. Ahmad, N. Raza, L. Zhang, Use of low-cost adsorbent for waste water treatment: recent progress, new trend and future perspectives, Desalin. Water Treat. 321 (2025) 100914, https://doi.org/10.1016/j.dwt.2024.100914.

[18] U. Tyagi, N. Anand, Sustainable and low-cost biomass derived adsorbents for the removal of toxic contaminants from wastewater: Approaches and future perspective, Waste Manag Bulletin of the Georgian Academy of Sciences 2 (2024) 308–325, https://doi.org/10.1016/j.wmb.2024.05.010.

[19] M. Nasrollahzadeh, M. Sajjadi, S. Iravani, R.S. Varma, Starch, cellulose, pectin, gum, alginate, chitin and chitosan derived (nano)materials for sustainable water treatment: a review, Carbohydr. Polym. 251 (2021) 116986, https://doi.org/10.1016/j.carbpol.2020.116986.

[20] A. Nayak, P. Chaudhary, B. Bhushan, K. Ghai, S. Singh, M. Sillanpää, Removal of emergent pollutants: a review on recent updates and future perspectives on polysaccharide-based composites vis-à-vis traditional adsorbents, Int. J. Biol. Macromol. 258 (2024) 129092, https://doi.org/10.1016/j.ijbiomac.2023.129092.

[21] A. Kumar, R. Indhur, A.G. Sheik, S.B.N. Krishna, S. Kumari, F. Bux, A review on conventional and novel adsorbents to boost the sorption capacity of heavy metals: current status, challenges and future outlook, Environ. Technol. Rev. 13 (2024) 521–543, https://doi.org/10.1080/21622515.2024.2377801.

[22] M.S. Akhtar, S. Ali, W. Zaman, Innovative adsorbents for pollutant removal: exploring the latest research and applications, Molecules 29 (2024), https://doi.org/10.3390/molecules29184317.

[23] N. Fijoł, A. Aguilar-Sánchez, A.P. Mathew, 3D-printable biopolymer-based materials for water treatment: a review, Chem. Eng. J. 430 (2022) 132964, https://doi.org/10.1016/j.cej.2021.132964.

[24] R. Scaffaro, E.F. Gulino, M.C. Citarrella, Multifunctional 3D-printed composites based on biopolymeric matrices and tomato plant (Solanum lycopersicum) waste for contextual fertilizer release and Cu(II) ions removal, Adv. Compos. Hybrid Mater. 7 (2024) 95, https://doi.org/10.1007/s42114-024-00908-4.

[25] R. Scaffaro, M.C. Citarrella, Stable and reusable electrospun bio-composite fibrous membranes based on PLA and natural fillers for air filtration applications, Sustain. Mater. Technol. 42 (2024) e01146, https://doi.org/10.1016/j.susmat.2024.e01146.

[26] M. Rajiv Gandhi, S. Meenakshi, Recent advancement in heavy metal removal onto silica based adsorbents and chitosan composites - a review, A B. Ion Exch. Adsorpt. Solvent Extr. (2013) 201–229.

[27] G.Z. Kyzas, M. Kostoglou, A.A. Vassiliou, N.K. Lazaridis, Treatment of real effluents from dyeing reactor: experimental and modeling approach by adsorption onto chitosan, Chem. Eng. J. 168 (2011) 577–585, https://doi.org/10.1016/j.cej.2011.01.026.

[28] D.A. Gkika, A.C. Mitropoulos, P. Kokkinos, D.A. Lambropoulou, I.K. Kalavrouziotis, D.N. Bikiaris, G.Z. Kyzas, Modified chitosan adsorbents in pharmaceutical simulated wastewaters: a review of the last updates, Carbohydr. Polym. Technol. Appl. 5 (2023) 100313, https://doi.org/10.1016/j.carpta.2023.100313.

[29] A. Balakrishnan, S. Appunni, M. Chinthala, M.M. Jacob, D.-V.-N. Vo, S.S. Reddy, E. S. Kunnel, Chitosan-based beads as sustainable adsorbents for wastewater remediation: a review, Environ. Chem. Lett. (2023), https://doi.org/10.1007/s10311-023-01563-9.

[30] M.A. Ahmed, A.A. Mohamed, The use of chitosan-based composites for environmental remediation: a review, Int. J. Biol. Macromol. 242 (2023) 124787, https://doi.org/10.1016/j.ijbiomac.2023.124787.

[31] M. Rajabi, S. Keihankhadiv, I. Suhas, R.R. Tyagi, M. Karri, N.M. Chaudhary, S. Mubarak, P. Chaudhary, P.S. Kumar, Comparison and interpretation of isotherm models for the adsorption of dyes, proteins, antibiotics, pesticides and heavy metal ions on different nanomaterials and non-nano materials—a comprehensive review, J. Nanostructure Chem. 13 (2023) 43–65, https://doi.org/10.1007/s40097-022-00509-x.

[32] V. Mishra, N. Mudgal, D. Rawat, P. Poria, P. Mukherjee, U. Sharma, P. Kumria, B. Pani, M. Singh, A. Yadav, F. Farooqi, R.S. Sharma, Integrating microalgae into textile wastewater treatment processes: advancements and opportunities, J. Water Process Eng. 55 (2023) 104128, https://doi.org/10.1016/j.jwpe.2023.104128.

[33] M. Al-Hammadi, M. Güngörmüşler, New insights into *Chlorella vulgaris* applications, Biotechnol. Bioeng. 121 (2024) 1486–1502, https://doi.org/10.1002/bit.28666.

[34] S. Mirizadeh, M. Pettinato, B. Fabiano, A. Converti, A.A. Casazza, Innovative treatment of digestate and biogas upgrade using Chlorella vulgaris, Chem. Eng. Trans. 105 (2023) 337–342, https://doi.org/10.3303/CET23105057.

[35] W. Liu, Q. Wang, H. Wang, Q. Xin, W. Hou, E. Hu, Z. Lei, Adsorption of uranium by chitosan/*Chlorella pyrenoidosa* composite adsorbent bearing phosphate ligand, Chemosphere 287 (2022) 132193, https://doi.org/10.1016/j.chemosphere.2021.132193.

[36] S. Mirizadeh, C. Solisio, A. Converti, A.A. Casazza, Efficient removal of tetracycline, ciprofloxacin, and amoxicillin by novel magnetic chitosan/microalgae biocomposites, Sep. Purif. Technol. (2023) 125115, https://doi.org/10.1016/j.seppur.2023.125115.

[37] E. Spennati, S. Mirizadeh, A.A. Casazza, C. Solisio, A. Converti, *Chlorella vulgaris* and *Arthrospira platensis* growth in a continuous membrane photobioreactor using industrial winery wastewater, Algal Res. 60 (2021) 102519, https://doi.org/10.1016/j.algal.2021.102519.

[38] M. Kates, B.E. Volcani, Lipid components of diatoms, Biochim. Biophys. Acta - Lipids Lipid Metab. 116 (1966) 264–278, https://doi.org/10.1016/0005-2760(66)90009-9.

[39] W. Tan, S. Lu, F. Liu, X. Feng, J.-Z. He, L. Koopal, Determination of the point-of-zero, charge of manganese oxides with different methods including an improved salt titration method, Soil Sci. 173 4 (2008) 173, https://doi.org/10.1097/SS.0b013e31816d1f12.

[40] M.H. Dehghani, A. Dehghan, H. Alidadi, M. Dolatabadi, M. Mehrabpour, A. Converti, Removal of methylene blue dye from aqueous solutions by a new chitosan/zeolite composite from shrimp waste: Kinetic and equilibrium study, Korean J. Chem. Eng. 34 (2017) 1699–1707, https://doi.org/10.1007/s11814-017-0077-2.

[41] E. Spennati, A.A. Casazza, A. Converti, G. Busca, Investigation on thermal pyrolysis of microalgae grown in winery wastewater: biofuels and chemicals production, Biomass Convers. Biorefinery. (2023), https://doi.org/10.1007/s13399-023-04118-8.

[42] S. Mirizadeh, S. Al Arni, M. Elwaheidi, A.A.M. Salih, A. Converti, A.A. Casazza, Adsorption of tetracycline and ciprofloxacin from aqueous solution on raw date palm waste, Chem. Eng. Technol. (2023), https://doi.org/10.1002/ceat.202300193.

[43] K. Althumayri, A. Guesmi, W.A. El-Fattah, A. Houas, N. Ben Hamadi, A. Shahat, Enhanced adsorption and evaluation of tetracycline removal in an aquatic system by modified silica nanotubes, ACS Omega 8 (2023) 6762–6777, https://doi.org/10.1021/acsomega.2c07377.

[44] T. Ahamad, M. Naushad, T. Al-Shahrani, N. Al-hokbany, S.M. Alshehri, Preparation of chitosan based magnetic nanocomposite for tetracycline adsorption: kinetic and thermodynamic studies, Int. J. Biol. Macromol. 147 (2020) 258–267, https://doi.org/10.1016/j.ijbiomac.2020.01.025.

[45] V. Son Tran, H. Hao Ngo, W. Guo, T. Ha Nguyen, T. Mai Ly Luong, X. Huan Nguyen, T. Lan Anh Phan, V. Trong Le, M. Phuong Nguyen, M. Khai Nguyen, New chitosan-biochar composite derived from agricultural waste for removing sulfamethoxazole antibiotics in water, Bioresour. Technol. 385 (2023) 129384, https://doi.org/10.1016/j.biortech.2023.129384.
[46] S. Chen, Z. Li, D. Yang, X. Qiu, D. Zheng, W. Liu, In situ synthesis of ZIF-8 on lignosulfonate functionalized polyethyleneimine/carboxymethyl chitosan hybrid aerogels for efficient tetracycline removal, Sep. Purif. Technol. 338 (2024) 126583, https://doi.org/10.1016/j.seppur.2024.126583.
[47] W. Xiang, Y. Wan, X. Zhang, Z. Tan, T. Xia, Y. Zheng, B. Gao, Adsorption of tetracycline hydrochloride onto ball-milled biochar: governing factors and mechanisms, Chemosphere 255 (2020) 127057, https://doi.org/10.1016/j.chemosphere.2020.127057.
[48] X.-L. Gong, H.-Q. Lu, K. Li, W. Li, Effective adsorption of crystal violet dye on sugarcane bagasse–bentonite/sodium alginate composite aerogel: characterisation, experiments, and advanced modelling, Sep. Purif. Technol. 286 (2022) 120478, https://doi.org/10.1016/j.seppur.2022.120478.
[49] A. Nasiri, S. Rajabi, A. Amiri, M. Fattahizade, O. Hasani, A. Lalehzari, M. Hashemi, Adsorption of tetracycline using CuCoFe2O4@Chitosan as a new and green magnetic nanohybrid adsorbent from aqueous solutions: isotherm, kinetic and thermodynamic study, Arab. J. Chem. 15 (2022) 104014, https://doi.org/10.1016/j.arabjc.2022.104014.
[50] S.M. Shalaby, F.F. Madkour, H.Y. El-Kassas, A.A. Mohamed, A.M. Elgarahy, Green synthesis of recyclable iron oxide nanoparticles using *Spirulina platensis* microalgae for adsorptive removal of cationic and anionic dyes, Environ. Sci. Pollut. Res. Int. 28 (2021) 65549–65572, https://doi.org/10.1007/s11356-021-15544-4.
[51] X. Zheng, C. Pan, S. Zheng, Y. Guo, Fmsunctionalized magnetic chitosan-based adsorbent for efficient tetracycline removal: deep investigation of adsorption behaviors and mechanis, Sep. Purif. Technol. 335 (2024) 126212, https://doi.org/10.1016/j.seppur.2023.126212.
[52] M. Massoudinejad, H. Rasoulzadeh, M. Ghaderpoori, Magnetic chitosan nanocomposite: fabrication, properties, and optimization for adsorptive removal of crystal violet from aqueous solutions, Carbohydr. Polym. 206 (2019) 844–853, https://doi.org/10.1016/j.carbpol.2018.11.048.
[53] Y. Liu, X. Zhang, L. Zhao, Removal of tetracycline from water using ethylenediamine-modified magnetic chitosan, Water Cycle 4 (2023) 179–191, https://doi.org/10.1016/j.watcyc.2023.09.001.
[54] T. He, X. Liu, S. Lv, D. Wei, L. Liu, Three-dimensional graded porous structure and compressible KGM-GO/CS/SA composite aerogel spheres for efficient adsorption of antibiotics, Sep. Purif. Technol. 346 (2024) 127547, https://doi.org/10.1016/j.seppur.2024.127547.
[55] A. Zubrik, M. Matik, E. Mačingová, Z. Danková, D. Jáger, J. Briančin, L. Machala, J. Pechoušek, S. Hredzák, The use of microwave irradiation for preparation and fast-acting regeneration of magnetic biochars, Chem. Eng. Process. - Process Intensif. 178 (2022) 109016, https://doi.org/10.1016/j.cep.2022.109016.
[56] C. Solisio, E. Spennati, A.A. Casazza, S. Arni, M.S. Alves Palma, A. Converti, Kinetics and isotherms of mercury biosorption by dry biomass of *Arthrospira* (*Spirulina*) *platensis*, Chem. Eng. Technol. 43 (2020) 240–247, https://doi.org/10.1002/ceat.201900463.
[57] R. Kamaraj, A. Pandiarajan, S. Jayakiruba, M. Naushad, S. Vasudevan, Kinetics, thermodynamics and isotherm modeling for removal of nitrate from liquids by facile one-pot electrosynthesized nano zinc hydroxide, J. Mol. Liq. 215 (2016) 204–211, https://doi.org/10.1016/j.molliq.2015.12.032.
[58] Z. Chai, C. Li, Y. Zhu, X. Song, M. Chen, Y.L. Yang, D. Chen, X. Liang, J. Wu, Arginine-modified magnetic chitosan: preparation, characterization and adsorption of gallic acid in sugar solution, Int. J. Biol. Macromol. 165 (2020) 506–516, https://doi.org/10.1016/j.ijbiomac.2020.09.141.
[59] A. Zanotti, L. Baldino, S. Cardea, E. Reverchon, Dye removal from wastewater using nanostructured chitosan aerogels produced by supercritical CO2 drying, J. Supercrit. Fluids. 216 (2025) 106442, https://doi.org/10.1016/j.supflu.2024.106442.
[60] Y.-M. Ge, X.-F. Zhao, J.-H. Xu, J.-Z. Liu, J.-S. Yang, S.-J. Li, Recyclable magnetic chitosan microspheres with good ability of removing cationic dyes from aqueous solutions, Int. J. Biol. Macromol. 167 (2021) 1020–1029, https://doi.org/10.1016/j.ijbiomac.2020.11.057.
[61] S.E.A. Elashery, M.M. El-Bouraie, E.A. Abdelgawad, N.F. Attia, G.G. Mohamed, Adsorptive performance of bentonite-chitosan nanocomposite as a dual antibacterial and reusable adsorbent for Reactive Red 195 and crystal violet removal: kinetic and thermodynamic studies, Biomass Convers. Biorefinery. 15 (2025) 2511–2524, https://doi.org/10.1007/s13399-023-05059-y.
[62] R. Ahmad, M.O. Ejaz, Efficient adsorption of crystal violet (CV) dye onto benign chitosan-modified l-cysteine/bentonite (CS-Cys/Bent) bionanocomposite: synthesis, characterization and experimental studies, Dye. Pigment. 216 (2023) 111305, https://doi.org/10.1016/j.dyepig.2023.111305.
[63] A.C. Khorasani, S.A. Shojaosadati, Magnetic pectin-*Chlorella vulgaris* biosorbent for the adsorption of dyes, J. Environ. Chem. Eng. 7 (2019) 103062, https://doi.org/10.1016/j.jece.2019.103062.
[64] A.S. Abdulhameed, A.H. Jawad, E. Kashi, K.A. Radzun, Z.A. ALOthman, L. D. Wilson, Insight into adsorption mechanism, modeling, and desirability function of crystal violet and methylene blue dyes by microalgae: Box-Behnken design application, Algal Res. 67 (2022) 102864, https://doi.org/10.1016/j.algal.2022.102864.
[65] U.A. Guler, M. Ersan, E. Tuncel, F. Dügenci, Mono and simultaneous removal of crystal violet and safranin dyes from aqueous solutions by HDTMA-modified *Spirulina* sp, Process Saf. Environ. Prot. 99 (2016) 194–206, https://doi.org/10.1016/j.psep.2015.11.006.
[66] S. Bhukal, A. Sharma, D. Rishi, S. Kumar, B. Deepak, K. Pal, S. Mona, *Spirulina* based iron oxide nanoparticles for adsorptive removal of crystal violet dye, TOPCatal. 65 (2022) 1675–1685, https://doi.org/10.1007/s11244-022-01640-3.
[67] R. Zhao, T. Ma, S. Zhao, H. Rong, Y. Tian, G. Zhu, Uniform and stable immobilization of metal-organic frameworks into chitosan matrix for enhanced tetracycline removal from water, Chem. Eng. J. 382 (2020) 122893, https://doi.org/10.1016/j.cej.2019.122893.
[68] X. Zheng, C. Pan, S. Zheng, Y. Guo, Functionalized magnetic chitosan-based adsorbent for efficient tetracycline removal: deep investigation of adsorption behaviors and mechanisms, Sep. Purif. Technol. 335 (2024), https://doi.org/10.1016/j.seppur.2023.126212.
[69] M. Shahmansoori, S. Yaghmaei, N.M. Mahmoodi, Green synthesis of chitosan-ZIF67 composite beads for efficient removal of Malachite Green and Tetracycline, Chem. Eng. Sci. 304 (2025) 121017, https://doi.org/10.1016/j.ces.2024.121017.
[70] Z. Li, H. Li, X. Zeng, S. Liu, Y. Yang, Adsorption and photodegradation of tetracycline by mannose-grafted chitosan composite films: performance, mechanism and availability, Chem. Eng. J. 458 (2023) 141455, https://doi.org/10.1016/j.cej.2023.141455.
[71] K. Valizadeh, A. Bateni, N. Sojoodi, R. Rafiei, A.H. Behroozi, A. Maleki, Preparation and characterization of chitosan-curdlan composite magnetized by zinc ferrite for efficient adsorption of tetracycline antibiotics in water, Int. J. Biol. Macromol. 235 (2023) 123826, https://doi.org/10.1016/j.ijbiomac.2023.123826.
[72] B. Chen, Y. Chen, Y. Cao, J. Huang, X. Chen, X. Pan, Collaboratively scavenge tetracycline and Cu2+ from their combined system by Fe3+-modified magnetic chitosan: performance, mechanisms, and dynamic sorption process, Chem. Eng. J. 484 (2024) 149625, https://doi.org/10.1016/j.cej.2024.149625.
[73] J. Liang, C. Li, S. Zhang, B.A. Mohamed, L. Wang, J. Xiang, S. Hu, Y. Wang, X. Hu, Activation of poplar and *spirulina* with H3PO4: marked influence of biological structures of the biomasses on evolution structure of activated carbon, Fuel Process. Technol. 252 (2023) 107986, https://doi.org/10.1016/j.fuproc.2023.107986.
[74] I. Abd, M. M-Ridha, Simultaneous adsorption of tetracycline and amoxicillin by *Cladophora* and *Spirulina* algae biomass, Iraqi, J. Agric. Sci. 52 (2021) 1290–1303, https://doi.org/10.36103/ijas.v52i5.1467.
[75] S. Mohamed Nasser, M. Abbas, M. Trari, Understanding the rate-limiting step adsorption kinetics onto biomaterials for mechanism adsorption control, Prog. React. Kinet. Mech. 49 (2024) 14686783241226858, https://doi.org/10.1177/14686783241226858.
[76] M. Masoudinia, P. Arabkhani, F. Sadegh, A. Asfaram, Synthesis and characterization of the magnetic chitosan/zinc oxide nanocomposite: an efficient magnetic adsorbent for removal of harmful aromatic micropollutants from wastewater, J. Mol. Struct. 1303 (2024) 137603, https://doi.org/10.1016/j.molstruc.2024.137603.
[77] X. Li, K. Li, J. Wu, B. Li, W. Wang, J. Tang, Facile preparation of sodium alginate gel beads enhanced by polyamino-modified 3D carbon for efficient remediation of organic dyes in wastewater, Sep. Purif. Technol. 339 (2024), https://doi.org/10.1016/j.seppur.2024.126637.
[78] A. Meas, E. Wi, M. Chang, H.S. Hwang, Carboxylmethyl cellulose produced from wood sawdust for improving properties of sodium alginate hydrogel in dye adsorption, Sep. Purif. Technol. 341 (2024), https://doi.org/10.1016/j.seppur.2024.126906.
[79] E.W.E.S. Shahrin, N.A.H. Narudin, N.N.M. Shahri, M. Nur, J.W. Lim, M.R. Bilad, A. H. Mahadi, J. Hobley, A. Usman, A comparative study of adsorption behavior of rifampicin, streptomycin, and ibuprofen contaminants from aqueous solutions onto chitosan: dynamic interactions, kinetics, diffusions, and mechanisms, Emerg. Contam. 9 (2023) 100199, https://doi.org/10.1016/j.emcon.2022.100199.
[80] K.Z. Elwakeel, A.A. Atia, E. Guibal, Fast removal of uranium from aqueous solutions using tetraethylenepentamine modified magnetic chitosan resin, Bioresour. Technol. 160 (2014) 107–114, https://doi.org/10.1016/j.biortech.2014.01.037.
[81] V. Rizzi, D. Lacalamita, J. Gubitosa, P. Fini, A. Petrella, R. Romita, A. Agostiano, J. A. Gabaldón, M.I. Fortea Gorbe, T. Gómez-Morte, P. Cosma, Removal of tetracycline from polluted water by chitosan-olive pomace adsorbing films, Sci. Total Environ. 693 (2019), https://doi.org/10.1016/j.scitotenv.2019.133620.
[82] A. Fathollahi, S.J. Coupe, A.H. El-Sheikh, L.A. Sañudo-Fontaneda, The biosorption of mercury by permeable pavement biofilms in stormwater attenuation, Sci. Total Environ. 741 (2020) 140411, https://doi.org/10.1016/j.scitotenv.2020.140411.
[83] Y. Wang, C. Wang, X. Huang, Q. Zhang, T. Wang, X. Guo, Guideline for modeling solid-liquid adsorption: kinetics, isotherm, fixed bed, and thermodynamics, Chemosphere 349 (2024) 140736, https://doi.org/10.1016/j.chemosphere.2023.140736.
[84] S. Rajabi, Z. Derakhshan, M. Hashemi, M. Feilizadeh, S. Heidari Kochaki, H. Hashemi, M. Salehi, A. Zare, N.S. Shourabi, S. Moradalizadeh, Metronidazole adsorption by bio-synthesized silver-zinc ferrite nanoadsorbent in presence of chitosan from aqueous media: response surface methodology, Appl. Water Sci. 14 (2024) 1–19, https://doi.org/10.1007/s13201-024-02152-z.